ACS APPLIED MATERIALS & INTERFACES

www.acsami.org

Research Article

# Targeted Delivery of a Matrix Metalloproteinases-2 Specific Inhibitor Using Multifunctional Nanogels to Attenuate Ischemic Skeletal Muscle Degeneration and Promote Revascularization

Yu Dang, Ning Gao, Hong Niu, Ya Guan, Zhaobo Fan, and Jianjun Guan*

Cite This: *ACS Appl. Mater. Interfaces* 2021, 13, 5907−5918

Read Online

ACCESS | Metrics & More | Article Recommendations

**ABSTRACT:** Critical limb ischemia (CLI) is a severe form of peripheral artery disease (PAD). It is featured by degenerated skeletal muscle and poor vascularization. During the development of CLI, the upregulated matrix metalloproteinase-2 (MMP-2) degrades muscle extracellular matrix to initiate the degeneration. Meanwhile, MMP-2 is necessary for blood vessel formation. It is thus hypothesized that appropriate MMP-2 bioactivity in ischemic limbs will not only attenuate muscle degeneration but also promote blood vessel formation. Herein, we developed ischemia-targeting poly(*N*-isopropylacrylamide)-based nanogels to specifically deliver an MMP-2 inhibitor CTTHWGFTLC (CTT) into ischemic limbs to tailor MMP-2 bioactivity. Besides acting as an MMP-2 inhibitor, CTT promoted endothelial cell migration under conditions mimicking the ischemic limbs. The nanogels were sensitive to the pH of ischemic tissues, allowing them to largely aggregate in the injured area. To help reduce nanogel uptake by macrophages and increase circulation time, the nanogels were cloaked with a platelet membrane. An ischemia-targeting peptide CSTSMLKA (CST) was further conjugated on the platelet membrane for targeted delivery of nanogels into the ischemic area. CTT gradually released from the nanogels for 4 weeks. The nanogels mostly accumulated in the ischemic area for 28 days. The released CTT preserved collagen in the muscle and promoted its regeneration. In addition, CTT stimulated angiogenesis. Four weeks after CLI, the blood flow and vessel density of the ischemic limbs treated with the nanogels were remarkably higher than the control groups without CTT release. These results demonstrate that the developed nanogel-based CTT release system has the potential to stimulate ischemic limb regeneration.

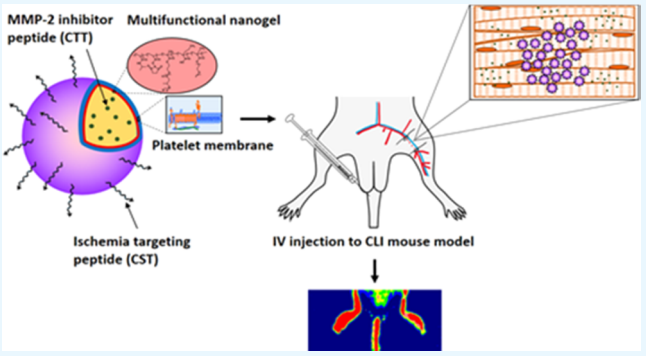


**KEYWORDS:** *critical limb ischemia, angiogenesis, targeted delivery, nanogel, MMP-2 inhibitor*



## INTRODUCTION

Peripheral artery disease (PAD) is a pathological condition caused by the narrowing of blood vessels. It affects ∼27 million people in North America.[1] Critical limb ischemia (CLI) represents the most severe case of PAD. It is characterized by degenerated skeletal muscle and poor vascularization. Regeneration of skeletal muscle and vasculature is crucial to prevent limb amputation.[1−4] However, current endovascular and surgical approaches and pharmacological treatments show limited efficacy.[3−9] Therefore, superior alternatives to current treatments are critically needed for CLI treatment. Herein, we aim to target matrix metalloproteinase-2 (MMP-2) in the ischemic limbs to simultaneously attenuate skeletal muscle degeneration and promote vessel regeneration.

Following PAD, MMPs, especially MMP-2, are upregulated.[3] The resulting imbalance between MMPs and the tissue inhibitors of metalloproteinase (TIMPs) leads to the extensive degradation of extracellular matrix (ECM) mainly collagens in the skeletal muscle. This initiates the skeletal muscle degeneration.[10] Therefore, a decrease of MMP-2 bioactivity will attenuate the degradation and preserve ECM architecture. In ischemic limb, MMP-2 is associated with angiogenesis. Knockout of MMP-2 in mice led to delayed angiogenesis.[11−13] An appropriate amount of MMP-2 allows to partially degrade ECM to give a path to endothelial cells for vessel formation. The ECM degradation also releases matrix-bound angiogenic growth factors such as vascular endothelial growth factor to facilitate vessel formation.[14−16] Thus, control of MMP-2 bioactivity will not only delay skeletal muscle degeneration but also promote vessel regeneration.

Received: October 27, 2020
Accepted: January 20, 2021
Published: January 28, 2021

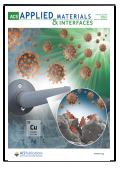

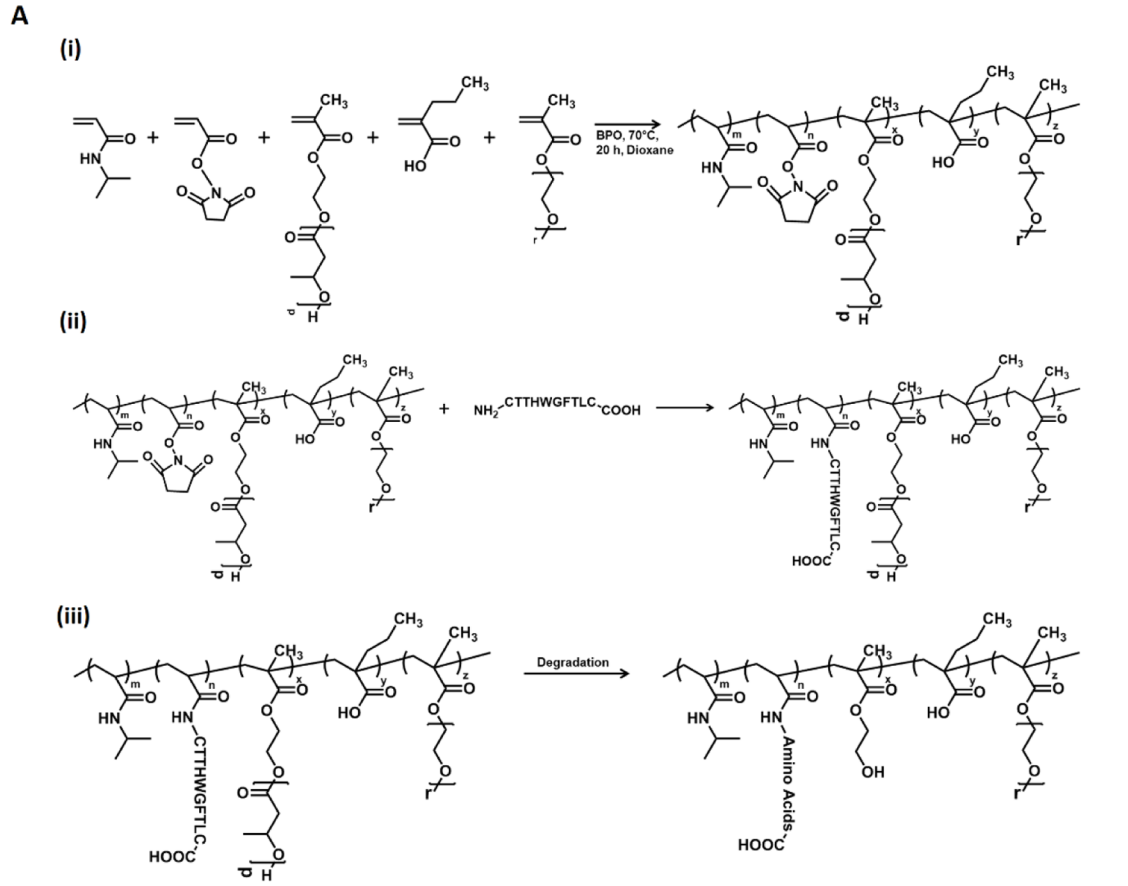


C

| Gel code name | Feed ratio* | Composition | LCST (°C) | Water content (%) | LCST of degradation product (°C) |
|---|---|---|---|---|---|
| PNNHPM1 | 50/15/25/5/5 | 40/14/32/8/6 | 10.4±0.4 | 44.2±1.4 | 66.6±1.7 |
| PNNHPM 2 | 50/10/25/10/5 | 48/5/28/12/6 | 10.3±0.2 | 40.7±4.2 | 68.0±0.8 |
| PNNHPM 3 | 45/15/25/5/10 | 39/12.5/27/8.5/13 | 10.1±0.1 | 92.3±11.4 | 75.4±1.4 |

**Figure 1.** (A) (i) Preparation of poly(NIPAAm-*co*-NAS-*co*-HEMA-HB4-*co*-PAA-*co*-MAPEG) via free radical polymerization. (ii) Reaction between PNNHPM and CTT. (iii) Degradation process of PNNHPM-CTT. (B) $^{1}$H NMR spectrum of poly(NIPAAm-*co*-NAS-*co*-HEMA-HB4-*co*-PAA-*co*-MAPEG). (C) Copolymer feed ratio, actual composition, LCST, water content, and LCST of degradation product. (*Ratio of NIPAAm/NAS/HEMA-HB4/PAA/MAPEG.) (D) Degradation of PNNHPM hydrogels over 4 weeks. (E) Cell cytotoxicity of supernatant from hydrogel polymers after 4 weeks' degradation (NS: $p > 0.05$).

To specifically modulate MMP-2 bioactivity, the use of MMP-2-specific inhibitors is an attractive approach as bioactivity of other MMPs will not be affected. Current MMP-2 specific inhibitors are predominately small organic molecules with reactive zinc-chelating groups.[17,18] One of the major concerns of these inhibitors is toxicity as the effective


https://dx.doi.org/10.1021/acsami.0c19271
ACS Appl. Mater. Interfaces 2021, 13, 5907−5918

dosage may exceed toxicity level.[19,20] This can be addressed using recombinant TIMPs and MMP-2 specific peptides.[21−23] It has recently been demonstrated that the MMP-2-specific peptide CTTHWGFTLC (CTT) successfully reduced MMP-2 bioactivity in the infarcted hearts and preserved cardiac ECM.[24] Unlike many other MMP-2-specific inhibitors, CTT does not affect cell attachment and spreading on the matrix.[23] We found in this work that CTT even promoted endothelial cell migration under TGF$\beta$ condition. TGF$\beta$ is upregulated in ischemic limbs, which inhibits endothelial cell migration.[25,26] We therefore encapsulated CTT into nanogels (NGs) for sustained release of CTT to control MMP-2 bioactivity. The nanogels were designed to specifically target ischemic skeletal muscle to decrease off-target effects. Systemic delivery without targeting capability may lead to CTT distributing to healthy tissue causing deleterious effects.

Nanogels have been extensively employed as delivery vehicles for small molecules, peptides, and proteins.[27,28] Because of their relatively high hydrophilicity, small and large molecules readily diffuse within the nanogels and release out. Nanogels can be administrated by minimally invasive intravenous (IV) injection and specifically accumulate in tissues of interest when designed to have targeting property.[29,30] Nanogels based on poly(*N*-isopropylacrylamide) (NIPAAm) and its derivatives have been widely used for drug delivery applications.[31−34] These polymers are not only thermosensitive but also highly biocompatible. The thermosensitivity allows to conveniently load drugs into nanogels at temperatures below their lower critical solution temperatures (LCSTs), although the drugs can also be loaded during nanogel fabrication.[35,36] In addition, the thermosensitivity enables to manipulate nanogel core−shell structure.[37] A potential disadvantage of these nanogels is that they cannot be readily removed from the body after drug release as most of them are not degradable or bioeliminable, and their LCSTs are typically lower than body temperature.[38−40] In this work, we have designed bioeliminable poly(*N*-isopropylacrylamide)-based nanogels with degradable side chains (Figure 1A(i)). The LCSTs were lower than 37 °C before the degradation of side chain and higher than 37 °C after degradation. Therefore, the thermosensitivity allows the nanogel to assume stable nanostructure at 37 °C before side-chain degradation. Following degradation (Figure 1A(iii)), the elevated LCSTs allow the nanogels to dissolve in body fluid and be eliminated from the body.

In this work, nanogels were also designed to be pH-sensitive with pH sensitivity between 6 and 7. This enables nanogels to aggregate specifically at the pH condition of ischemic areas (pH ∼ 6−7).[41] The platelet membrane was used to cloak nanogels to increase their circulation time and reduce the uptake of nanogels by cells like macrophages. A peptide CSTSMLKA (CST) that can specifically target ischemic regions was also conjugated on the surface of the platelet membrane. The in vitro results showed that the encapsulated CTT can release sustainably for 28 days. The in vivo results demonstrated that multifunctional nanogels exhibited excellent targeting capability, had a long retention time, attenuated muscle degeneration, and accelerated revascularization in the ischemic limbs.

## MATERIALS AND METHODS

**Materials.** *N*-Isopropylacrylamide (NIPAAm) was purchased from TCI America and was recrystallized three times in hexane before use. Poly(ethylene glycol) methacrylate (MAPEG) and 2-hydroxyethyl methacrylate (HEMA) were purchased from VWR. $NH_2$-C-T-T-H-W-G-F-T-L-C-K (FITC)-COOH (CTT) and $NH_2$-K (rhodamine B)-C-S-T-S-M-L-K-A-COOH (CST) were synthesized by Celtek Bioscience, LLC. Bovine blood was purchased from Quad Five.

**Synthesis of Hydrogels.** *N*-Acryloxysuccinimide (NAS), 2-hydroxyethyl methacrylate-oligo($\beta$-hydroxybutyrate) (HEMAOHB), and propylacrylic acid (PAA) were synthesized following previously established procedures.[32,42,43] Oligo($\beta$-hydroxybutyrate) had average of four $\beta$-hydroxybutyrate units. Poly(NIPAAm-*co*-NAS-*co*-HEMAOHB-*co*-PAA-*co*-MAPEG) (PNNHPM) was synthesized using benzoyl peroxide (BPO) as an initiator (Figure 1A). Monomers with designated feed ratios (NIPAAm/NAS/HEMAOHB/PAA/MAPEG = 50/15/25/5/5, 50/10/25/10/5, or 45/15/25/5/10) were first dissolved in dioxane under nitrogen. BPO (0.2 mol %) was then added, and the mixture was heated at 70 °C for 20 h. Upon completion, the reaction mixture was poured into a large volume of cold hexane to precipitate the polymer. The crude product was purified by dissolving in tetrahydrofuran (THF) and precipitating into cold ethyl ether. The final product was collected by filtration and dried in a vacuum oven. $^1$H NMR spectrum was used to confirm the polymer structure and calculate the composition. The degradation product of the hydrogel polymer Poly(NIPAAm-*co*-NAS-*co*-HEMA-*co*-PAA-*co*-MAPEG) was synthesized using the same method as described above.

**Characterization of Hydrogels.** The lower critical solution temperature (LCST) of the hydrogel solution and the degradation product of hydrogel were characterized using differential scanning calorimetry (DSC) with a temperature range of 0−60 and 30−80 °C and a heating rate of 10 °C/min. Water content was measured by first dissolving the hydrogels in dichloromethane (DCM) to make a 10% solution, and then 0.2 mL of the solution was transferred to each small centrifuge tube. After the solvent evaporation, 0.2 mL of Dulbecco's phosphate-buffered saline (DPBS) was added to each sample, and the samples ($n$ = 3) were incubated at 37 °C for 24 h. The samples were decanted and lyophilized. The water content was determined by calculating the weight difference between lyophilized mass ($w_1$) and wet mass ($w_2$).

$$\text{water content} = \frac{w_2 - w_1}{w_1} \times 100\% \quad (1)$$

The degradation study was conducted in a 37 °C water bath for 8 weeks. The solid hydrogel membranes that formed after evaporation of the DCM were weighed ($w_4$) and then immersed in DPBS. Samples ($n$ = 4) were taken out at designated intervals, lyophilized, and weighed ($w_3$). The weight remaining was calculated as follows

$$\text{weight remaining} = \frac{w_3}{w_4} \times 100\% \quad (2)$$

**Hydrogel Degradation Product Cytotoxicity.** To test the cytotoxicity of the degradation product of the hydrogels, the degradation medium during the degradation test was collected and sterilized by UV light and filtered through 220 nm sterile filters. Rat cardiac fibroblast cells were seeded in a 96-well plate at a density of 50 000 cells/well. After 24 h of culture in an incubator (37 °C, 5% $CO_2$), 20 $\mu$L of degradation medium was added to 200 $\mu$L of culture medium. 3-(4,5-Dimethylthiazol-2-yl)-2,5-diphenyltetrazolium bromide (MTT) solution was then added after another 24 h of culture. The medium was then discarded after 4 h of incubation, and 200 $\mu$L of dimethyl sulfoxide (DMSO) was added to each well. An optical density (OD) reading was obtained using a SpectraMax iD3 multimode microplate reader after all of the precipitates in the well were fully dissolved. The results were normalized to the control group, where 20 $\mu$L of DPBS was added instead of degradation medium.

**Fabrication of Nanogels.** Nanogels based on the synthesized hydrogels were fabricated following an adapted procedure.[44] The hydrogel was first dissolved in THF at a concentration of 0.1% w/v. The solution was quickly dropped into a solution of THF and DPBS,


https://dx.doi.org/10.1021/acsami.0c19271
ACS Appl. Mater. Interfaces 2021, 13, 5907−5918

then maintained under constant ultrasonication for 10 min. The THF was removed by air blowing, and the nanogel emulsion was concentrated to 1 mg/mL. The pH sensitivity of the nanogel was tested using dynamic light scattering (DLS) (Malvern Panalytical) under pH 7.4 and 6.5, respectively.

**Isolation of the Platelet Membrane and Fabrication of Platelet Membrane-Coated Nanogels (PMNG).** The platelet membrane was extracted from fresh bovine blood through at least three repeated freeze−thaw cycles.[45] After being washed with DPBS containing protease inhibitor followed by centrifugation, the platelet membrane pellet was suspended in DPBS and sonicated using a sonicator (Fisher Scientific). For platelet membrane cloaking, ~$2 \times 10^9$ platelets were mixed with 1 mg of nanogel under sonication for 2 min. The structure of platelet membrane-coated nanogels (abbreviated as PMNG) was examined by transmission electron microscopy (TEM) (FEI Tecnai G2 Spirit TEM) after negative staining with uranyl acetate. The size and $\zeta$ potential change after platelet membrane cloaking were monitored using DLS.

The ischemia-targeting peptide, CST, was conjugated onto the surface of PMNG using a crosslinker, disuccinimidyl suberate (DSS, ThermoFisher Scientific). CST and PMNG were first mixed in monosodium phosphate buffer. DSS solution in DMSO (50 mM) was then added. The mixture was incubated at room temperature for 30 min with constant stirring. The reaction was quenched with excess glycine for 15 min, and the nonreacted reagent was removed by dialysis.

**Testing Cell Uptake of PMNG.** Human cardiac microvascular endothelial cells (HMVECs) and bone marrow-derived macrophages (BMMs) were seeded onto glass slides in 24-well plates with a density of $5.0 \times 10^4$ cells/well. The cells were incubated for 24 h before the addition of PMNG. To image the PMNG, rhodamine-B-labeled CST was conjugated to the PMNG surface. After 2 h of incubation, the samples ($n = 3$) were fixed with 4% paraformaldehyde solution. F-actin and 4′,6-diamidino-2-phenylindole (DAPI) stainings were then performed. The images were taken by a confocal microscope (Olympus FV 1000). The cellular uptake in each image was quantified as follows

$$\text{cell uptake rate} = \frac{\text{no. of cells with PMNP}}{\text{no. of total cells}} \times 100\% \quad (3)$$

**Blood Compatibility of PMNG.** The blood compatibility of PMNG was tested following the kinetic method with modification.[46,47] Bovine blood (0.2 mL) and 0.1 M $CaCl_2$ (0.03 mL) were placed in a 1.5 mL centrifuge tube at 37 °C. Typically, 1 mg/mL PMNG (0.125 mL) or phosphate-buffered saline (PBS) (0.125 mL) was then added followed by mixing using a vortex mixer. At each predetermined time point, the specimen ($n = 3$) was transferred into 50 mL of DI water and incubated for 5 min. The concentration of hemoglobin in the water that was released from free red blood cells not trapped in a thrombus was measured by a SpectraMax iD3 multimode microplate reader at 540 nm.

**Loading CTT into Nanogels and Monitoring CTT Release.** CTT was loaded in nanogels during the fabrication. CTT was first dissolved in DMSO to make a 3 mg/mL solution and then added into the hydrogel solution. After mixing, 300 $\mu g_{CTT}/mg_{Hydrogel}$ solution was quickly added to a mixture of THF and DPBS with constant ultrasonication for 10 min. The remaining THF in the nanogel emulsion was removed by air blowing, and the excessive CTT was removed by Vivaspin molecular weight cutoff (MWCO) 5000 centrifuge tubes. The CTT release study was performed by dialyzing 400 $\mu$L of CTT nanogel emulsion, using 3.5k MWCO Slide-A-Lyzers against DPBS for 28 days. Fluorescein isothiocyanate (FITC)-labeled CTT was used to spectrometrically determine the release kinetics of CTT peptide encapsulated in nanogels. At each time point, 1.2 mL of dialysate was collected and the same amount of fresh release medium (PBS) was added. The fluorescent intensity of released CTT was measured by a SpectraMax iD3 multimode microplate reader. An excitation wavelength of 495 nm and an emission wavelength of 518 nm were used. The CTT concentrations before and after dialysis at each time point were determined according to a standard curve established using the same fluorescence reading parameters ($n = 4$). The CTT loading efficiency was calculated as follows

$$\text{CTT loading efficiency} = \frac{C_{CTT}V_{NP}}{w_{total,0}} \times 100\% \quad (4)$$

where $C_{CTT}$ is the CTT concentration before dialysis, $V_{NP}$ is the volume of the nanoparticle solution, and $w_{total,0}$ is the total weight of CTT used initially.

**In Vitro HMVEC Migration.** To study the migration of HMVEC in response to CTT, the cells were seeded into six-well plates ($n = 3$ for each group). The cells were cultured to high confluency, and the cell monolayer was scratched with a sterile 200 $\mu$L pipette tip. The culture medium was replaced with serum-free media. TGF$\beta$1 and CTT were added to the medium at 5 ng/mL and 100 $\mu$g/mL, respectively. The images of HMVECs were taken at 0 and 24 h after treatment. The migrated area was quantified using ImageJ.

**Ischemic Limb Surgery and the Intravenous (IV) Injection of Nanogels.** Animal surgeries were performed following guidelines approved by the Institutional Animal Care and Use Committee of The Ohio State University. Eight-week-old female C57BL/6 mice were first anesthetized using 2% isoflurane, and then hindlimb ischemia was induced by surgical ligation of the unilateral femoral artery and vein according to our previous study.[34] The contralateral hindlimb was used as control. One day after the induction of ischemia, IV injections were made through the tail vein (150 $\mu$L/injection, 3 mg/mL PMNG (or PMNG/CTT) in sterile PBS). The injected groups included PMNG and PMNG loaded with CTT (PMNG/CTT group). Mice with surgically induced hindlimb ischemia were used as the control (surgery group). Four mice were used for laser Doppler perfusion imaging in each group, and three mice were used for IVIS imaging at each time point.

**Laser Doppler Perfusion Imaging.** Blood perfusion in the ischemic limbs was monitored using a laser Doppler perfusion imager (Perimed) at 1, 7, 14, 21, and 28 days after IV injection ($n = 4$). The blood flow ratio of ischemia/normal limb was calculated by comparing the perfusion intensity in the ischemic region to the intensity in a contralateral normal limb region with the same area.[48]

**IVIS Imaging for Tracking Nanaogels.** To monitor the targeting capability of the PMNG, an in vivo imaging system (IVIS) (Lumina II, PerkinElmer) was used. At days 1, 7, 14, 21, and 28 after IV injection, three mice were euthanized. The hindlimbs, heart, liver, lung, spleen, and kidneys were harvested. Fluorescent images were taken with an excitation of 535 nm and a DsRed emission filter to collect the fluorescence signal of rhodamine. The fluorescent intensity at each limb was calculated using PerkinElmer Living Image software.[49]

**Histological Analyses.** Four weeks after IV injection, healthy and ischemic hindlimbs, liver, lung, and kidney of the mice were harvested and fixed using 4% paraformaldehyde. The tissues were embedded in paraffin and sectioned with a thickness of 5 $\mu$m. The hindlimb sections were stained with hematoxylin and eosin (H&E) and Picrosirius red (PSR). The total collagen, type I collagen, and type III collagen content were quantified from PSR staining imaged under polarized light. Type I collagen was determined as the yellow-red area in PSR staining under polarized light, and type III collagen was determined as the green area in PSR staining under polarized light. Masson's trichrome staining was used for liver, lung, and kidney.

To perform immunohistochemical staining, deparaffinized tissue sections were blocked with serum and incubated with primary antibodies against F4/80, $\alpha$-smooth muscle actin ($\alpha$-SMA), or isolectin. F4/80 and $\alpha$-SMA were used to stain macrophage and smooth muscle cells, respectively. Isolectin, a dye that specifically binds to terminal $\alpha$-galactosyl residues expressed by endothelial cells, was used to stain endothelial cells in the blood vessels.[50] Alexa Fluor 488 and Alexa Fluor 647 were used as secondary antibodies. Cell nuclei were stained with Hoechst 33342 or DAPI. Images of stained sections were taken using an Olympus FV 1000 confocal microscope. Isolectin positive lumens were recognized as blood vessels. The mature vessels were $\alpha$-SMA and isolectin positive lumens.


https://dx.doi.org/10.1021/acsami.0c19271
ACS Appl. Mater. Interfaces 2021, 13, 5907−5918

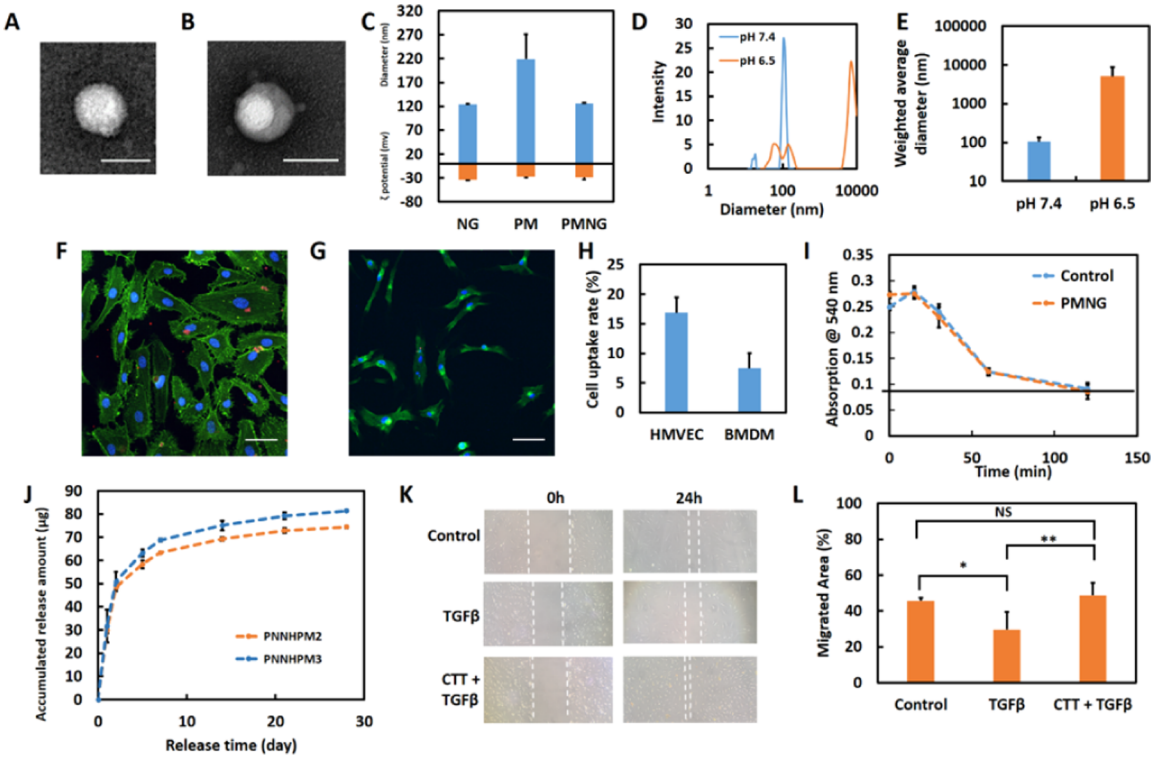


**Figure 2.** (A) TEM image of NG, and (B) TEM image of PMNG, both negatively stained with 1% uranyl acetate (scale bar = 50 nm). (C) DLS results showing size and ζ potential of nanogels (NG), platelet membrane (PM), and PMNG. (D) DLS results showing size change of NG under different pH. (E) Weighted average diameter of NG under different pH. (F) Cell uptake of PMNG in HMVEC. (G) Cell uptake of PMNG in BMDM (scale bar = 50 μm). (H) Quantification of cell uptake rate. (I) Blood compatibility test of PMNG. (J) Release kinetics of CTT-FITC encapsulated in different types of hydrogel NGs (CTT concentration 300 μg/mg). (K) In vitro cell migration study of HMVEC using wound closure model. (L) Quantified migrated area during the first 24 h of the migration study. (*: $p < 0.05$, **: $p < 0.01$).

**Statistical Analyses.** Statistical analysis was performed using one-way analysis of variance (ANOVA) with post hoc Tukey test. Statistical significance was defined as $p < 0.05$.

## RESULTS AND DISCUSSION

**Synthesis and Characterization of Thermo- and pH-Sensitive Hydrogels.** The hydrogels used for nanogel fabrication were synthesized by free radical polymerization of *N*-isopropylacrylamide (NIPAAm), *N*-acryloxysuccinimide (NAS), 2-hydroxyethyl methacrylate-oligo(β-hydroxybutyrate) (HEMAOHB), propylacrylic acid (PAA), and poly(ethylene glycol) methacrylate (MAPEG). $^1$H NMR spectra confirmed the structure of the hydrogels. A representative spectrum shown in Figure 1B exhibited characteristic peaks corresponding to NIPAAm (a), NAS (b), HEMAOHB (g), PAA (d), and MAPEG (e and f). The calculated composition of each hydrogel was consistent with the feed ratio (Figure 1C). The NIPAAm component provided the hydrogels with thermal sensitivity, allowing the fabricated nanogels to be stable at 37 °C without the need for chemical crosslinking. NAS component in the hydrogels was used to react with CTT (Figure 1A(ii)). The immobilized CTT can interact with free CTT so as to increase its interaction with nanogel, facilitating long-term CTT release. The HEMAOHB component had a degradable and hydrophobic side-chain oligo(β-hydroxybutyrate). This can be used to tune hydrogel LCST before and after degradation. Before degradation, the hydrophobic oligomer imparted hydrogels with low LCSTs, ∼10 °C (Figure 1C), enabling the nanogels to be stable at 37 °C. Following the degradation of oligomer, the hydrogels became more hydrophilic (Figure 1A(iii)). This elevated the LCSTs well above 37 °C (Figure 1C). Thus, the final degradation products can dissolve in body fluid and be removed from the body. The PAA has a p$K_a$ value of ∼6.3,[51] allowing the hydrogels to have pH-responsive range of 6−7, within the range of ischemic tissue.[41] The MAPEG component was used to adjust the overall hydrophilicity of the hydrogel.

The water content of the hydrogels was in the range of 41−92% depending on the ratio of hydrophilic MAPEG (Figure 1C). The hydrogels (PNNHPM1 and PNNHPM2) with a MAPEG ratio of 5% had similar water content, ∼40%. The increase of the ratio to 10% (hydrogel PNNHPM3) significantly augmented the water content to 92%. The hydrogels gradually lost weight after being incubated in the 37 °C PBS for 4 weeks (Figure 1D). The remaining weights were above 80%. The hydrogel with the highest water content exhibited the greatest weight loss, possibly because the higher water content accelerated the hydrolytic degradation process.[52] To determine biocompatibility of the degradation products, the degradation medium at week 4 was added to the cardiac fibroblast culture medium. After 24 h, the cell viability (MTT assay) in groups with degradation products did not show a significant difference from the control group without degradation products ($p > 0.05$), demonstrating that the hydrogels were biocompatible (Figure 1E).

**Fabrication and Characterization of Nanogels.** Three types of nanogels encapsulated with CTT were fabricated using the three hydrogels synthesized above. To reduce immune rejection following intravenous injection of nanogels, and increase their circulation time, the platelet membrane was


https://dx.doi.org/10.1021/acsami.0c19271
ACS Appl. Mater. Interfaces 2021, 13, 5907−5918

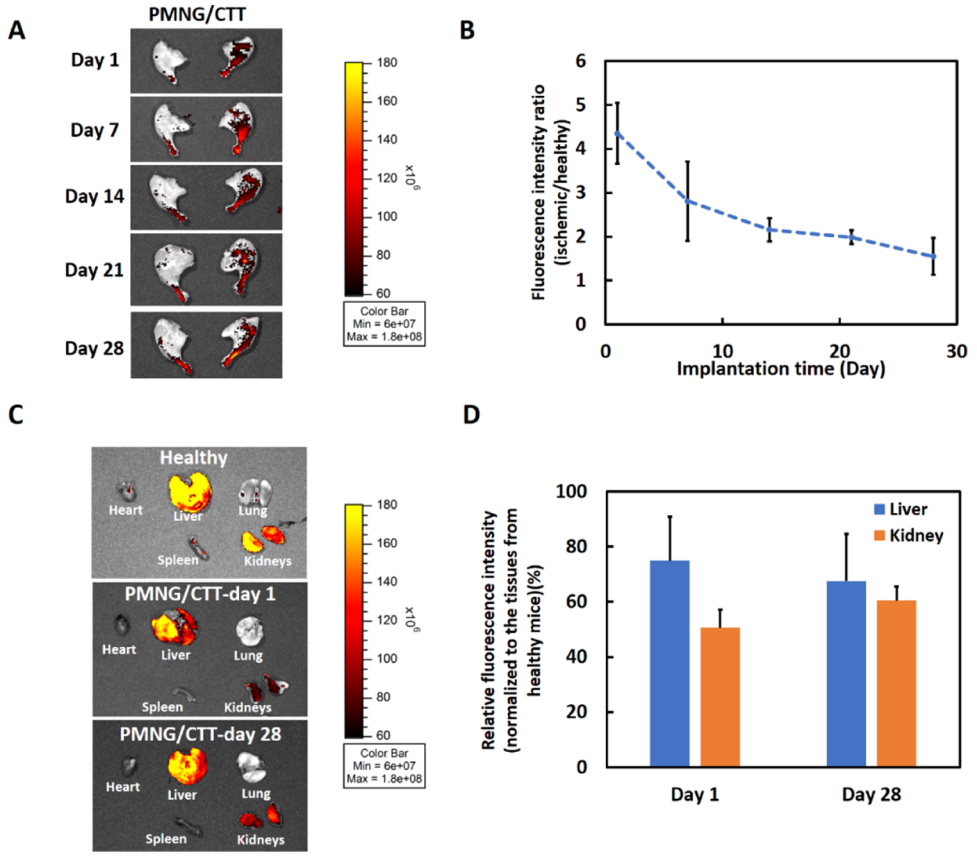


**Figure 3.** (A) IVIS images of ischemic mouse hindlimb at different time points for PMNG/CTT group. (B) Quantification of IVIS rhodamine fluorescence intensity ratio in PMNG/CTT group. (C) Ex vivo whole organ IVIS imaging of rhodamine B signal on day 1 and day 28 post injection. (D) Relative fluorescence intensity of liver and kidneys from PMNG/CTT group normalized to the tissues from healthy mice.

cloaked onto the nanogel surface. Previous studies have demonstrated that platelet membrane (not live prothrombotic platelet) increases nanoparticles' circulation time.[45,53] The platelet membrane also has the innate ability to find injured endothelial cells by binding motifs on the membrane.[54,55] Therefore, the platelet membrane-cloaked nanogels can target ischemic tissues. To enhance the targeting capability, ischemia-targeting peptide CST[56,57] (labeled with rhodamine) was conjugated on the platelet membrane. The TEM images of the nanogel (NG) and platelet membrane-cloaked nanogel (PMNG) confirmed the successful cloaking of the platelet membrane (Figure 2A,B). After cloaking, the size remained almost the same (Figure 2C). Meanwhile, the $\zeta$ potential increased from ∼−34 to ∼−29 mV, tending to carry the same electrical charge as the platelet membrane (Figure 2C).

After the platelet membrane-cloaked nanogels are accumulated at the ischemic region, the platelet membrane may be dissolved by enzymatic digestion and/or lipid transport[58,59] and left with bare nanogels. To ensure that these nanogels remain in the ischemic area for a long period, the hydrogels used for nanogels were designed to have a PAA component. It becomes more hydrophobic at the pH of the ischemic tissue (6−7), leading to the nanogel aggregation in the tissue. Larger-size aggregates can retain in the tissue longer, resulting from decreased cellular uptake and reduced possibility of being flushed away.[60] At pH 7.4, the nanogels exhibited a diameter of ∼120 nm (Figure 2D,E). At pH 6.5, the nanogels were aggregated, and the diameter was increased significantly to ∼5000 nm ($p < 0.0001$, Figure 2D,E).

**Cellular Uptake and Blood Compatibility of Nanogels.** After being delivered in vivo, the nanogels may be uptaken by cells in the ischemic limb. To determine the cellular uptake of PMNGs, human cardiac microvascular endothelial cell (HMVEC) and bone marrow-derived macrophage (BMM) were used. PMNGs exhibited relatively low cellular uptake in both cell types where 16.8% of HMVECs and 7.5% of BMMs had nanogels inside after 2 h of incubation (Figure 2F−H). These results were consistent with previous studies that demonstrated that platelet membrane cloaking can decrease cellular uptake.[45] One of the concerns when using the platelet membrane is that it may promote blood clot, preventing the nanogels from accumulating in the ischemic limbs. To determine the blood compatibility of PMNGs, bovine blood and PMNGs were incubated together, and the concentration of hemoglobin released from free red blood cells was measured spectroscopically ($n = 3$). The bovine blood incubated with PBS was used as control. Higher absorbance reading of hemoglobin (540 nm) indicates better thromboresistance.[47] The PMNG group displayed similar absorbance as the PBS group (Figure 2I), demonstrating that PMNGs possessed excellent thromboresistance.

**CTT Loading Efficiency and In Vitro CTT Release from Nanogels.** CTT was encapsulated in the nanogels with a loading efficiency of 41.0% for PNNHPM1, 42.5% for PNNHPM2, and 41.7% for PNNHPM3. The nanogels fabricated using three different hydrogels showed similar loading efficiency. CTT was able to gradually and continuously release from PMNGs over the course of 4 weeks (Figure 2J).


https://dx.doi.org/10.1021/acsami.0c19271
ACS Appl. Mater. Interfaces 2021, 13, 5907−5918

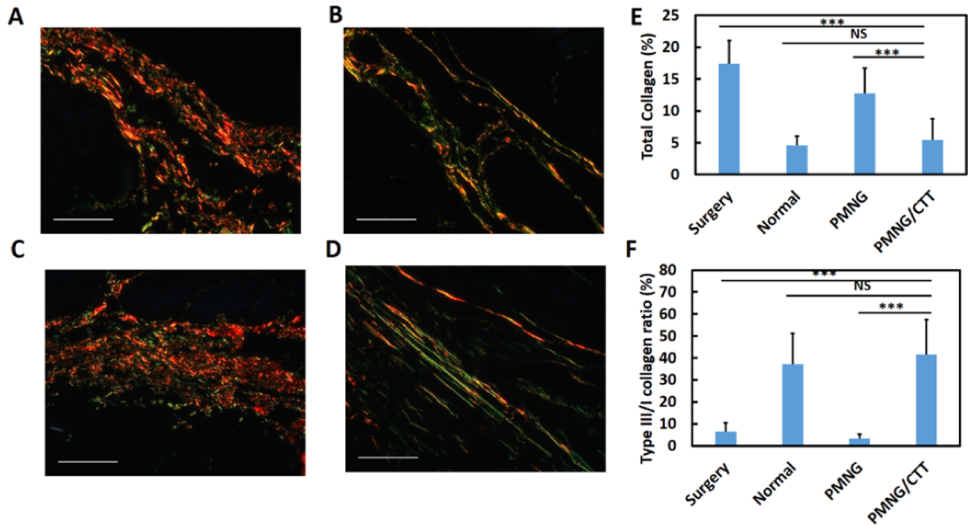


**Figure 4.** Picrosirius red staining of ischemic limbs 28 days after injection: (A) ischemic limb from surgery group (Surgery), (B) normal limb from surgery group (Normal), (C) PMNG group, and (D) PMNG/CTT group. (E) Quantification of total collagen content. (F) Quantification of type III/I ratio (scale bar = 50 $\mu$m) (***$p$ <0.0001, NS: $p > 0.05$).

To determine how nanogels' water content affected CTT release, PMNGs fabricated from hydrogels with largely different water content (PNNHPM2 and PNNHPM3) were used. CTT underwent a burst release for the first 2 days, followed by a slower and sustained release from day 2 to day 28. The sustained release is possibly due to hydrogen bonding between the hydrogel and CTT, and the interaction between CTT immobilized to the hydrogel and free CTT. The CTT release kinetics was related to the water content of the hydrogel used for nanogel fabrication (Figure 2J). The PMNGs fabricated from higher water content PNNHPM3 released significantly greater CTT than those fabricated from lower water content PNNHPM2 from day 5 to day 28 ($p <$ 0.05 at each time point). It is possible that higher water content promoted faster diffusion of CTT to the surrounding environment.

**CTT Promoted Endothelial Cell Migration in the TGF$\beta$-Rich Environment.** Besides acting as a MMP-2 inhibitor, CTT had a positive effect on endothelial cell migration under TGF$\beta$ condition existing in the ischemic limbs (Figure 2K,L). TGF$\beta$ expression is upregulated in ischemic limbs.[25,26] A monolayer scratch assay was used to determine HMVEC migration ($n$ = 3 for each group). Compared with the control group without TGF$\beta$, the group with TGF$\beta$ exhibited slower cell migration at 24 h ($p < 0.05$), indicating that TGF$\beta$ inhibited HMVEC migration. The addition of CTT reversed the inhibitive effect of TGF$\beta$. The cell migration was significantly increased at 24 h ($p < 0.01$). No significant difference was found between the group with CTT and TGF$\beta$ and the control group without TGF$\beta$ ($p > 0.05$). The above results demonstrate that CTT has the potential to promote angiogenesis in ischemic limbs. CTT has been found previously to inhibit endothelial cell migration in the absence of TGF$\beta$.[23] The finding in this work reveals that the combination of CTT and TGF$\beta$ can promote endothelial cell migration.

**Targeting Capability of Nanogels.** To test the efficacy of the PMNG-based CTT delivery system in vivo, we induced hindlimb ischemia in mice, and PMNGs were injected through the tail vein after 24 h (150 $\mu$L per animal, $n$ = 4 for the control group, $n$ = 19 for PMNG and PMNG/CTT groups, respectively). IVIS imaging was used to determine the accumulation of nanoparticles in hindlimbs with or without ischemia (Figure 3A,B). In nanogels, both CST and platelet membrane had targeting capability. CST targets the ischemic environment.[56,57] It was initially discovered by in vivo phage display although the precise mechanism by which it targets ischemia is still unclear.[56] Platelet membrane targets injured endothelial cells.[54,55] After 1 day of IV injection, PMNG/CTT nanogels mostly accumulated in the ischemic hindlimb (right) instead of healthy hindlimb (left), proving that nanogels had the excellent capability of targeting ischemic area. The nanogels remained predominately in the ischemic hindlimbs after 7, 14, 21, and 28 days of post injection. These results demonstrate that PMNG/CTT nanogels had long-term retention capability. Previous studies have shown that nanogels with sizes ranging from 15 to 350 nm are often cleared from the body within 24 h.[61] In this work, nanogels had a similar size. The long retention time of the PMNG/CTT nanogels is likely resulted from dual targeting properties (ischemia and injured endothelial cells).

To investigate the possible accumulation of off-target nanogels in major organs, IVIS images of heart, liver, lungs, kidney, and spleen were taken ex vivo 1 and 28 days post injection for the PMNG/CTT group (Figure 3C). The heart, lung, and spleen from healthy mice (no injection) and the PMNG/CTT group showed similar fluorescence signals at both time points. Notably, the liver and kidney in the PMNG/CTT group had lower fluorescence intensities than those from the healthy mice at both time points (Figure 3D). These results demonstrate that nanogels had minimum off-target effect.

**Released CTT Preserved ECM in Ischemic Limbs.** To evaluate the efficacy of CTT delivery in preserving ECM in the ischemic hindlimbs, Picrosirius red (PSR) staining was performed on the ischemic limbs 4 weeks after treatment to determine total collagen content and ratio of types I and III collagen (Figure 4A–F). The total collagen content in the PMNG/CTT group was ~5.5%, similar to that in the normal hindlimbs ($p > 0.05$, Figure 4E). In addition, collagen type III/


https://dx.doi.org/10.1021/acsami.0c19271
ACS Appl. Mater. Interfaces 2021, 13, 5907–5918

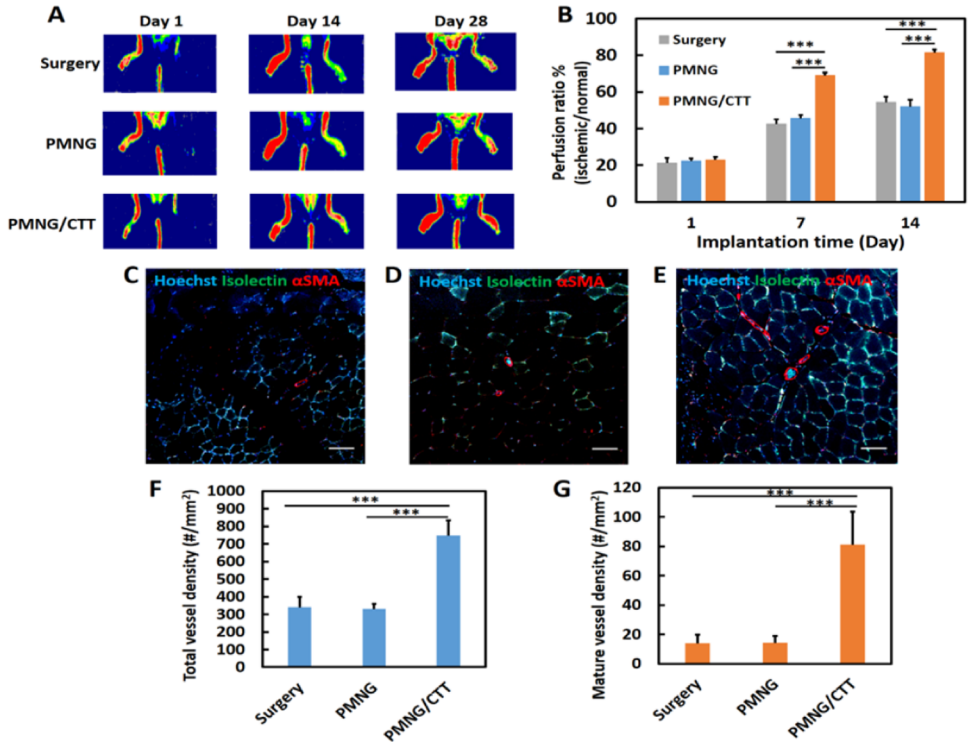


**Figure 5.** Blood perfusion tests of ischemic limbs at day 1, day 14, and day 28 for Surgery group, PMNG group, and PMNG/CTT group, respectively. (A) Laser Doppler perfusion images and (B) ratios of blood perfusion at different time points. $\alpha$-SMA and isolectin staining of ischemic limb from (C) Surgery group, (D) PMNG group, (E) PMNG/CTT group (scale bar = 50 $\mu$m), (F) quantification of total blood vessels, and (G) quantification of mature blood vessels (***$p < 0.0001$).

I ratio was similar in the PMNG/CTT group and the normal hindlimb tissue ($p > 0.05$, Figure 4F). Types I and III collagen are two abundant components of the ECM in the hindlimbs.[62] The adverse tissue remodeling in the ischemic hindlimbs leads to the formation of scar tissue rich in type I collagen and with lower type III/I ratio.[63] In this work, the PMNG/CTT group had a similar type III/I ratio as the normal hindlimbs (~40%). The surgery group and PMNG group exhibited a much lower type III/I ratio (<10%). The above results demonstrate that the delivered CTT successfully preserved ECM in the ischemic limbs, while scar tissue was formed in the surgery and PMNG groups. One of the concerns to use MMP-2 inhibitors is the possible occurrence of fibrosis. First, MMP-2 inhibitors may stimulate the differentiation of fibroblasts into myofibroblasts,[24] which are known as the predominant contributor of type I collagen.[64] Second, the inhibition of MMP-2 by the delivered CTT may break the local balance of MMP-2 and the TIMPs in the ischemic limbs, leading to overproduction of collagen. Our results demonstrate that the dosage of delivered CTT was appropriate, and it did not induce fibrosis.

The ischemic limbs without treatment (surgery group) and treated with PMNGs (PMNG group) exhibited similar total collagen content at day 28 ($p > 0.05$, Figure 4E). These values were significantly greater than those in the ischemic limbs treated with CTT ($p < 0.0001$). In addition, the type III/I collagen ratio in the surgery and PMNG groups were similar and significantly lower than that in the PMNG/CTT group ($p < 0.0001$, Figure 4F). These results demonstrate that ischemic limbs without CTT treatment developed fibrosis at day 28. Fibrotic tissue is rich in type I collagen. The above results are consistent with a previous report using a mouse ischemic hindlimb model.[65] Active MMP-2 is upregulated in ischemic limbs during the first 2 weeks.[66] It is possible that the upregulated MMP-2 degraded ECM initially. The collagen I was then oversecreted when the MMP-2 expression was not upregulated.

**Released CTT Ameliorated Angiogenesis in Ischemic Limbs.** CTT was able to promote endothelial cell migration under TGF$\beta$ condition existing in ischemic limbs (Figure 2K,L). To determine whether delivered CTT promoted angiogenesis, a Perimed laser Doppler perfusion imager was used to measure blood perfusion (Figure 5A). In the surgery group and PMNG group, the blood perfusion was slowly increased with ~50% recovery after 4 weeks. The injection of CTT encapsulated PMNGs (PMNG/CTT group) significantly increased blood perfusion, achieving 81.3% of recovery ($p < 0.0001$, Figure 5B). The recovery rate in the first 2 weeks was faster than that in the weeks 2−4. This is possibly related to the higher release rate of CTT in the first 2 weeks.

The ameliorated angiogenesis was further confirmed by vessel density in ischemic limbs (Figure 5C−G). Four weeks after injection, the blood vessel density in the surgery and PMNG groups was similar ($p > 0.05$). The delivery of CTT remarkably increased blood vessel density. The density was more than 2.2 times of the surgery and PMNG groups ($p < 0.0001$, Figure 5F). The delivered CTT also promoted vessel maturation (Figure 5G). The $\alpha$SMA + and Isolectin + mature vessel density in the PMNG/CTT group was ~5.8 times of the surgery and PMNG groups ($p < 0.0001$, PMNG/CTT vs PMNG, PMNG/CTT vs surgery). The above results demonstrate that the use of CTT to stimulate endothelial cell migration and attenuate MMP-2 bioactivity successfully stimulated vessel regeneration in ischemic limbs. MMPs and TIMPs often play complex roles in angiogenesis. The


https://dx.doi.org/10.1021/acsami.0c19271
ACS Appl. Mater. Interfaces 2021, 13, 5907−5918

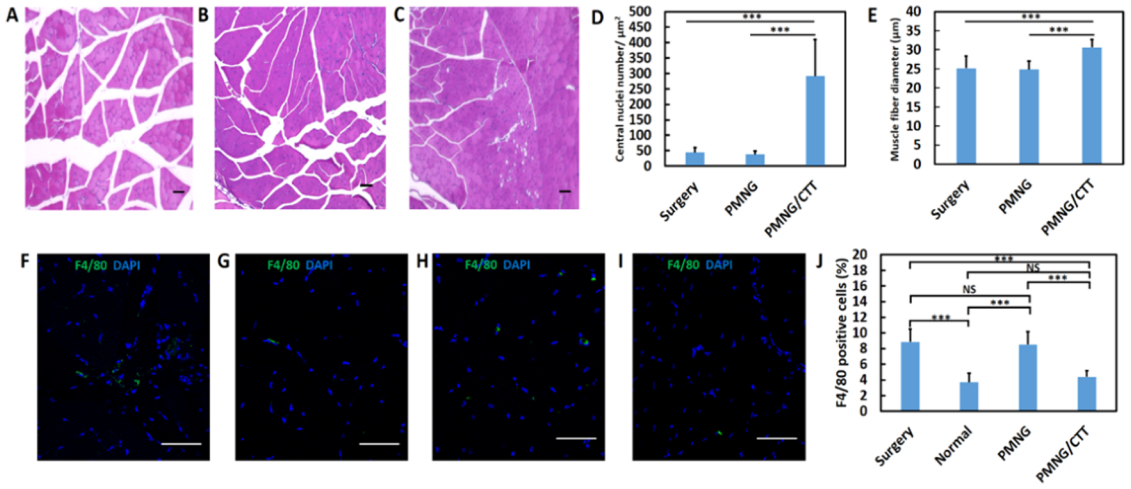


**Figure 6.** H&E staining of ischemic limbs 28 days after injection: (A) Surgery group, (B) PMNG group, and (C) PMNG/CTT group. Scale bar = 50 $\mu$m. (D) quantification of central nuclei numbers. (E) quantification of muscle fiber diameters. F4/80 staining of (F) ischemic limb from surgery group (Surgery), (G) normal limb from surgery group (Normal), (H) ischemic limb from PMNG group, (G) ischemic limb from PMNG/CTT group (scale bar = 50 $\mu$m), and (J) quantification of F4/80 positive cells (%) (***$p$ < 0.0001, NS: $p$ > 0.05).

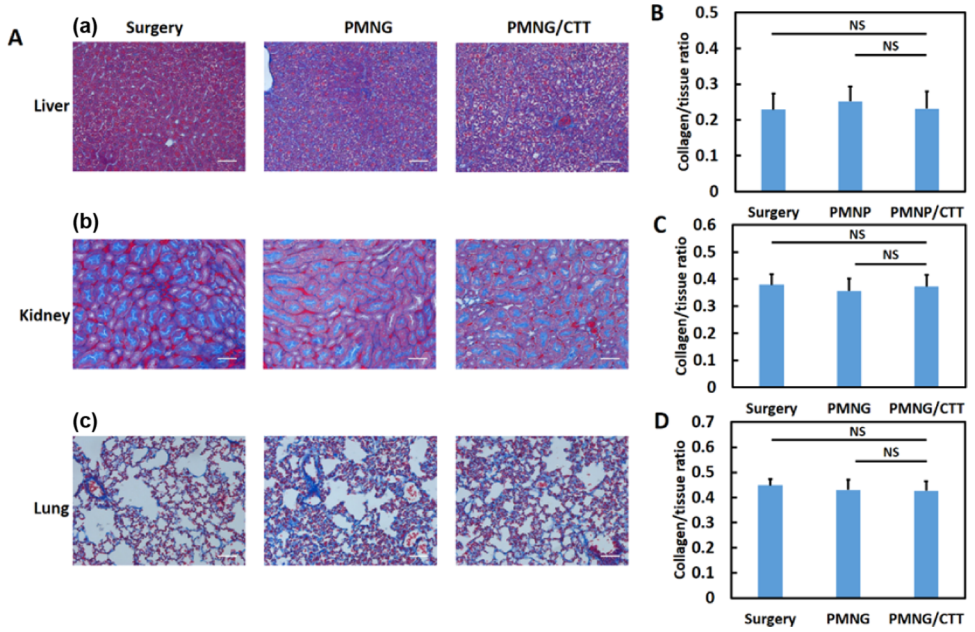


**Figure 7.** (A) Masson's trichrome staining images of liver (a), kidney (b), and lung (c) from surgery, PMNG, and PMNG/CTT groups, respectively (Scale bar = 50 $\mu$m). Quantification of collagen/muscle ratios for (B) liver, (C) kidney, and (D) lung (NS: $p$ > 0.05).

degradation of ECM by MMPs is crucial for the migration of endothelial cells.[16] On the other hand, excessive proteolytic cleavage of ECM has been shown to inhibit angiogenesis.[67,68] Our results show that the PMNG/CTT released appropriate amount of CTT to modulate MMP-2 bioactivity and angiogenesis.

**Released CTT Promoted Skeletal Muscle Regeneration in Ischemic Limbs.** Skeletal muscle regeneration was enhanced along with accelerated angiogenesis in ischemic limbs. The H&E image of ischemic limbs at day 28 demonstrated that remarkable muscle degeneration occurred in the surgery group without treatment, where the muscle fibers were highly isolated (Figure 6A). Injection of PMNGs without CTT did not inhibit degeneration (Figure 6B). In contrast, the injection of PMNG/CTT largely prevented the muscle fiber from separation (Figure 6C). The number of central nuclei and changes in muscle fiber diameter are important indicators of muscle regeneration. The PMNG/CTT group exhibited remarkably higher numbers of central nuclei (Figure 6D) and significantly larger muscle fiber diameters (Figure 6E) than the surgery and PMNG groups ($p$ < 0.0001). The enhanced muscle regeneration is likely resulted from the decreased MMP-2 bioactivity by released CTT. This led to the preservation of ECM (Figure 4), which provides three-dimensional (3D) structural support for skeletal muscle cells to proliferate and differentiate.[10] The muscle regeneration can also be attributed to the accelerated angiogenesis. The functional blood vessels supply oxygen and nutrient for the survival and proliferation of skeletal muscle cells.[69] Overall, the controlled delivery of CTT stimulated not only angiogenesis but also skeletal muscle regeneration in ischemic limbs.


https://dx.doi.org/10.1021/acsami.0c19271
ACS Appl. Mater. Interfaces 2021, 13, 5907−5918

**Released CTT Mitigated Inflammation in Ischemic Limbs.** Tissue inflammation was characterized in terms of the presence of F4/80 + macrophages in ischemic limbs (Figure 6F–J). After 28 days of injection, ischemic limbs without treatment (surgery group) and treated with PMNGs (PMNG group) had similar F4/80 + macrophage density ($p > 0.05$). This value was significantly greater than that in the normal limbs without surgery (normal group; $p < 0.0001$ for surgery vs normal, and PMNG vs normal). The PMNG/CTT group displayed a decreased amount of F4/80 + cells ($p < 0.0001$ for PMNG/CTT vs surgery, and PMNG/CTT vs PMNG), similar to the level in the normal limb ($p > 0.05$). These results demonstrate that the CTT released from PMNG/CTT largely reduced tissue inflammation. The attenuation of macrophage density in ischemic limbs is possibly the result of decreased MMP-9 bioactivity. CTT is specific to both MMP-2 and MMP-9. A previous study found that MMP-9 deficiency impaired the recruitment of proinflammatory macrophages into kidney.[70] In this work, the bovine platelet membrane was used in mice. However, it did not induce substantial inflammation (Figure 6F–J). In the future clinical studies, platelet membranes may be extracted from the patient's own blood, thus eliminating the potential risk of an immune response.

**Released CTT Did Not Cause Fibrosis in Liver, Kidney, and Lung.** One of the concerns when systemically delivering CTT is that off-targeted CTT may accumulate in the healthy organs and decrease their MMP-2 bioactivity, leading to tissue fibrosis. To determine whether major organs such as liver, kidney, and lung developed fibrosis after 4 weeks of injection of nanogels with or without CTT, Masson's trichrome staining was performed (Figure 7A–D). No significant difference in the collagen/tissue ratio was found among the surgery, PMNG, and PMNG/CTT groups for all three organs ($p > 0.05$), indicating that these organs did not develop fibrosis. These results also demonstrate that the off-target effect of the CTT was minimal if any. It is likely resulted from targeting capability of the developed nanogels.

## CONCLUSIONS

Thermal- and pH-sensitive nanogels camouflaged with the platelet membrane and conjugated with ischemia-targeting peptide were developed to deliver MMP-2 inhibitor CTT into ischemic limbs. The sustained release of CTT in nanogels was achieved for 28 days. The nanogels were able to target the ischemic region and remained in the tissue for at least 28 days. The amount of released CTT was appropriate for the simultaneous preservation of ECM in ischemic limbs, acceleration of angiogenesis and skeletal muscle regeneration, and decrease of tissue inflammation.

## AUTHOR INFORMATION


### Corresponding Author

**Jianjun Guan** − *Department of Mechanical Engineering and Materials Science, Washington University in St. Louis, St. Louis, Missouri 63130, United States; Department of Materials Science and Engineering, The Ohio State University, Columbus, Ohio 43210, United States;* orcid.org/0000-0002-1040-3386; Phone: 314-935-3537; Email: jguan22@wustl.edu

### Authors

**Yu Dang** − *Department of Mechanical Engineering and Materials Science, Washington University in St. Louis, St. Louis, Missouri 63130, United States; Department of Materials Science and Engineering, The Ohio State University, Columbus, Ohio 43210, United States*

**Ning Gao** − *Department of Mechanical Engineering and Materials Science, Washington University in St. Louis, St. Louis, Missouri 63130, United States; Department of Materials Science and Engineering, The Ohio State University, Columbus, Ohio 43210, United States*

**Hong Niu** − *Department of Mechanical Engineering and Materials Science, Washington University in St. Louis, St. Louis, Missouri 63130, United States; Department of Materials Science and Engineering, The Ohio State University, Columbus, Ohio 43210, United States*

**Ya Guan** − *Department of Mechanical Engineering and Materials Science, Washington University in St. Louis, St. Louis, Missouri 63130, United States; Department of Materials Science and Engineering, The Ohio State University, Columbus, Ohio 43210, United States*

**Zhaobo Fan** − *Department of Materials Science and Engineering, The Ohio State University, Columbus, Ohio 43210, United States*

Complete contact information is available at: https://pubs.acs.org/10.1021/acsami.0c19271


### Author Contributions

The manuscript was written through the contributions of all authors. All authors have given approval to the final version of the manuscript.


### Funding

This work was supported by U.S. National Institutes of Health (R01HL138175, R01HL138353, R01EB022018, R01AG056919, and R01AR077616) and National Science Foundation (1922857).


### Notes

The authors declare no competing financial interest.

## ACKNOWLEDGMENTS

We thank Drs. Haichang Li and Shengcai Wei for their help during the experiment. Confocal images were performed in part through the use of Washington University Center for Cellular Imaging (WUCCI) supported by Washington University School of Medicine, The Children's Discovery Institute of Washington University and St. Louis Children's Hospital (CDI-CORE-2015-505 and CDI-CORE-2019-813), and the Foundation for Barnes-Jewish Hospital (3770 and 4642).

## REFERENCES


(1) Alev, C.; Ii, M.; Asahara, T. Endothelial Progenitor Cells: A Novel Tool for the Therapy of Ischemic Diseases. *Antioxid. Redox Signaling* **2011**, 949.

(2) Benoit, E.; O'Donnell, T. F.; Patel, A. N. Safety and Efficacy of Autologous Cell Therapy in Critical Limb Ischemia: A Systematic Review. *Cell Transplant.* **2013**, 545.

(3) Gupta, N. K.; Armstrong, E. J.; Parikh, S. A. The Current State of Stem Cell Therapy for Peripheral Artery Disease. *Curr. Cardiol. Rep.* **2014**, No. 447.

(4) Raval, Z.; Losordo, D. W. Cell Therapy of Peripheral Arterial Disease: From Experimental Findings to Clinical Trials. *Circ. Res.* **2013**, 1288.

(5) Bradbury, A. W.; Adam, D. J.; Bell, J.; Forbes, J. F.; Fowkes, F. G. R.; Gillespie, I.; Ruckley, C. V.; Raab, G. M. Bypass versus Angioplasty in Severe Ischaemia of the Leg (BASIL) Trial: A Survival Prediction Model to Facilitate Clinical Decision Making. *J. Vasc. Surg.* **2010**, 52S.
(6) Cooke, J. P.; Losordo, D. W. Modulating the Vascular Response to Limb Ischemia: Angiogenic and Cell Therapies. *Circ. Res.* **2015**, 1561.
(7) Jazwa, A.; Florczyk, U.; Grochot-Przeczek, A.; Krist, B.; Loboda, A.; Jozkowicz, A.; Dulak, J. Limb Ischemia and Vessel Regeneration: Is There a Role for VEGF? *Vasc. Pharmacol.* **2016**, *86*, 18−30.
(8) Kitrou, P.; Karnabatidis, D.; Brountzos, E.; Katsanos, K.; Reppas, L.; Spiliopoulos, S. Gene-Based Therapies in Patients with Critical Limb Ischemia. *Expert Opin. Biol. Ther.* **2017**, *17*, 449−456.
(9) Suzuki, J. I.; Shimamura, M.; Suda, H.; Wakayama, K.; Kumagai, H.; Ikeda, Y.; Akazawa, H.; Isobe, M.; Komuro, I.; Morishita, R. Current Therapies and Investigational Drugs for Peripheral Arterial Disease. *Hypertens. Res.* **2016**, 183.
(10) Carmeli, E.; Moas, M.; Reznick, A. Z.; Coleman, R. Matrix Metalloproteinases and Skeletal Muscle: A Brief Review. *Muscle Nerve* **2004**, *29*, 191−197.
(11) Itoh, T.; Ikeda, T.; Gomi, H.; Nakao, S.; Suzuki, T.; Itohara, S. Unaltered Secretion of Beta-Amyloid Precursor Protein in Gelatinase A (Matrix Metalloproteinase 2)-Deficient Mice. *J. Biol. Chem.* **1997**, *272*, 22389−22392.
(12) Vu, T. H.; Shipley, J. M.; Bergers, G.; Berger, J. E.; Helms, J. A.; Hanahan, D.; Shapiro, S. D.; Senior, R. M.; Werb, Z. MMP-9/Gelatinase B Is a Key Regulator of Growth Plate Angiogenesis and Apoptosis of Hypertrophic Chondrocytes. *Cell* **1998**, *93*, 411−422.
(13) Itoh, T.; Tanioka, M.; Yoshida, H.; Yoshioka, T.; Nishimoto, H.; Itohara, S. Reduced Angiogenesis and Tumor Progression in Gelatinase A-Deficient Mice. *Cancer Res.* **1998**, *58*, 1048−1051.
(14) Bergers, G.; Brekken, R.; McMahon, G.; Vu, T. H.; Itoh, T.; Tamaki, K.; Tanzawa, K.; Thorpe, P.; Itohara, S.; Werb, Z.; Hanahan, D. Matrix Metalloproteinase-9 Triggers the Angiogenic Switch during Carcinogenesis. *Nat. Cell Biol.* **2000**, 737.
(15) Carmeliet, P. Mechanisms of Angiogenesis and Arteriogenesis. *Nat. Med.* **2000**, 389.
(16) Siefert, S. A.; Sarkar, R. Matrix Metalloproteinases in Vascular Physiology and Disease. *Vascular* **2012**, *20*, 210−216.
(17) Beckett, R. P.; Davidson, A. H.; Drummond, A. H.; Huxley, P.; Whittaker, M. Recent Advances in Matrix Metalloproteinase Inhibitor Research. *Drug Discovery Today* **1996**, 16.
(18) Talbot, D. C.; Brown, P. D. Experimental and Clinical Studies on the Use of Matrix Metalloproteinase Inhibitors for the Treatment of Cancer. *Eur. J. Cancer* **1996**, *32*, 2528−2533.
(19) Hudson, M. P.; Armstrong, P. W.; Ruzyllo, W.; Brum, J.; Cusmano, L.; Krzeski, P.; Lyon, R.; Quinones, M.; Theroux, P.; Sydlowski, D.; Kim, H. E.; Garcia, M. J.; Jaber, W. A.; Weaver, W. D. Effects of Selective Matrix Metalloproteinase Inhibitor (PG-116800) to Prevent Ventricular Remodeling After Myocardial Infarction: Results of the PREMIER (Prevention of Myocardial Infarction Early Remodeling) Trial. *J. Am. Coll. Cardiol.* **2006**, *48*, 15−20.
(20) Guo, Y.-H.; Gao, W.; Li, Q.; Li, P.-F.; Yao, P.-Y.; Chen, K. Tissue Inhibitor of Metalloproteinases-4 Suppresses Vascular Smooth Muscle Cell Migration and Induces Cell Apoptosis. *Life Sci.* **2004**, *75*, 2483−2493.
(21) Eckhouse, S. R.; Purcell, B. P.; McGarvey, J. R.; Lobb, D.; Logdon, C. B.; Doviak, H.; O'Neill, J. W.; Shuman, J. A.; Novack, C. P.; Zellars, K. N.; Pettaway, S.; Black, R. A.; Khakoo, A.; Lee, T.; Mukherjee, R.; Gorman, J. H.; Gorman, R. C.; Burdick, J. A.; Spinale, F. G. Local Hydrogel Release of Recombinant TIMP-3 Attenuates Adverse Left Ventricular Remodeling after Experimental Myocardial Infarction. *Sci. Transl. Med.* **2014**, *6*, No. 223ra21.
(22) Purcell, B. P.; Lobb, D.; Charati, M. B.; Dorsey, S. M.; Wade, R. J.; Zellars, K. N.; Doviak, H.; Pettaway, S.; Logdon, C. B.; Shuman, J. A.; Freels, P. D.; Gorman, J. H., 3rd; Gorman, R. C.; Spinale, F. G.; Burdick, J. A. Injectable and Bioresponsive Hydrogels for On-Demand Matrix Metalloproteinase Inhibition. *Nat. Mater.* **2014**, *13*, 653−661.
(23) Koivunen, E.; Arap, W.; Valtanen, H.; Rainisalo, A.; Medina, O. P.; Heikkilä, P.; Kantor, C.; Gahmberg, C. G.; Salo, T.; Konttinen, Y. T.; Sorsa, T.; Ruoslahti, E.; Pasqualini, R. Tumor Targeting with a Selective Gelatinase Inhibitor. *Nat. Biotechnol.* **1999**, *17*, 768−774.
(24) Fan, Z.; Fu, M.; Xu, Z.; Zhang, B.; Li, Z.; Li, H.; Zhou, X.; Liu, X.; Duan, Y.; Lin, P. H.; Duann, P.; Xie, X.; Ma, J.; Liu, Z.; Guan, J. Sustained Release of a Peptide-Based Matrix Metalloproteinase-2 Inhibitor to Attenuate Adverse Cardiac Remodeling and Improve Cardiac Function Following Myocardial Infarction. *Biomacromolecules* **2017**, *18*, 2820−2829.
(25) Goumans, M. J.; Valdimarsdottir, G.; Itoh, S.; Lebrin, F.; Larsson, J.; Mummery, C.; Karlsson, S.; ten Dijke, P. Activin Receptor-like Kinase (ALK)1 Is an Antagonistic Mediator of Lateral TGFbeta/ALK5 Signaling. *Mol. Cell* **2003**, *12*, 817−828.
(26) Goumans, M.-J.; Valdimarsdottir, G.; Itoh, S.; Rosendahl, A.; Sideras, P.; ten Dijke, P. Balancing the Activation State of the Endothelium via Two Distinct TGF-Beta Type I Receptors. *EMBO J.* **2002**, *21*, 1743−1753.
(27) Motornov, M.; Roiter, Y.; Tokarev, I.; Minko, S. Stimuli-Responsive Nanoparticles, Nanogels and Capsules for Integrated Multifunctional Intelligent Systems. *Prog. Polym. Sci.* **2010**, *35*, 174−211.
(28) Molina, M.; Asadian-Birjand, M.; Balach, J.; Bergueiro, J.; Miceli, E.; Calderon, M. Stimuli-Responsive Nanogel Composites and Their Application in Nanomedicine. *Chem. Soc. Rev.* **2015**, *44*, 6161−6186.
(29) Jin, G.-Z.; Chakraborty, A.; Lee, J.-H.; Knowles, J. C.; Kim, H.-W. Targeting with Nanoparticles for the Therapeutic Treatment of Brain Diseases. *J. Tissue Eng.* **2020**, *11*, No. 2041731419897460.
(30) Rosenblum, D.; Joshi, N.; Tao, W.; Karp, J. M.; Peer, D. Progress and Challenges towards Targeted Delivery of Cancer Therapeutics. *Nat. Commun.* **2018**, *9*, No. 1410.
(31) Cui, Z.; Lee, B. H.; Pauken, C.; Vernon, B. L. Degradation, Cytotoxicity and Biocompatibility of NIPAAm-Based Thermosensitive, Injectable and Bioresorbable Polymer Hydrogels. *J. Biomed. Mater. Res., Part A* **2012**, *98*, 159−166.
(32) Li, Z.; Fan, Z.; Xu, Y.; Lo, W.; Wang, X.; Niu, H.; Li, X.; Xie, X.; Khan, M.; Guan, J. PH-Sensitive and Thermosensitive Hydrogels as Stem-Cell Carriers for Cardiac Therapy. *ACS Appl. Mater. Interfaces* **2016**, *8*, 10752−10760.
(33) Li, T. S.; Cheng, K.; Malliaras, K.; Smith, R. R.; Zhang, Y.; Sun, B.; Matsushita, N.; Blusztajn, A.; Terrovitis, J.; Kusuoka, H.; Marbán, L.; Marbán, E. Direct Comparison of Different Stem Cell Types and Subpopulations Reveals Superior Paracrine Potency and Myocardial Repair Efficacy with Cardiosphere-Derived Cells. *J. Am. Coll. Cardiol.* **2012**, *59*, 942−953.
(34) Xu, Y.; Fu, M.; Li, Z.; Fan, Z.; Li, X.; Liu, Y.; Anderson, P. M.; Xie, X.; Liu, Z.; Guan, J. A Prosurvival and Proangiogenic Stem Cell Delivery System to Promote Ischemic Limb Regeneration. *Acta Biomater.* **2016**, *31*, 99−113.
(35) Sun, Q.; Deng, Y. Encapsulation of Polystyrene Latex with Temperature-Responsive Poly(N-Isopropylacrylamide) via a Self-Assembling Approach and the Adsorption Behaviors Therein. *Langmuir* **2005**, *21*, 5812−5816.
(36) Ivanov, A. E.; Ekeroth, J.; Nilsson, L.; Mattiasson, B.; Bergenståhl, B.; Galaev, I. Y. Variations of Wettability and Protein Adsorption on Solid Siliceous Carriers Grafted with Poly(N-Isopropylacrylamide). *J. Colloid Interface Sci.* **2006**, 538.
(37) Deloney, M.; Smart, K.; Christiansen, B. A.; Panitch, A. Thermoresponsive, Hollow, Degradable Core-Shell Nanoparticles for Intra-Articular Delivery of Anti-Inflammatory Peptide. *J. Controlled Release* **2020**, 47.
(38) De, P.; Gondi, S. R.; Sumerlin, B. S. Folate-Conjugated Thermoresponsive Block Copolymers: Highly Efficient Conjugation and Solution Self-Assembly. *Biomacromolecules* **2008**, *9*, 1064−1070.
(39) Li, G.; Song, S.; Guo, L.; Ma, S. Self-Assembly of Thermo- and PH-Responsive Poly(Acrylic Acid)-b-Poly(N-Isopropylacrylamide) Micelles for Drug Delivery. *J. Polym. Sci., Part A: Polym. Chem.* **2008**, 5028.


https://dx.doi.org/10.1021/acsami.0c19271
ACS Appl. Mater. Interfaces 2021, 13, 5907−5918

(40) Prazeres, T. J. V.; Farinha, J. P. S.; Martinho, J. M. G. Control of Oligonucleotide Distribution on the Shell of Thermo-Responsive Polymer Nanoparticles. *J. Phys. Chem. C* **2008**, *112*, 16331−16339.
(41) Hagberg, H. Intracellular PH during Ischemia in Skeletal Muscle: Relationship to Membrane Potential, Extracellular PH, Tissue Lactic Acid and ATP. *Pflügers Arch. Eur. J. Physiol.* **1985**, 342.
(42) D'Agosto, F.; Charreyre, M.-T.; Pichot, C. Side-Product of N-Acryloyloxysuccinimide Synthesis or Useful New Bifunctional Monomer? *Macromol. Biosci.* **2001**, *1*, 322−328.
(43) Li, Z. Development of Multi-Functional Stem Cell Delivery Systems for Cardiac Therapy. Dissertation, Graduate School of the Ohio State University, 2012.
(44) Yin, C.; Zhen, X.; Zhao, H.; Tang, Y.; Ji, Y.; Lyu, Y.; Fan, Q.; Huang, W.; Pu, K. Amphiphilic Semiconducting Oligomer for Near-Infrared Photoacoustic and Fluorescence Imaging. *ACS Appl. Mater. Interfaces* **2017**, *9*, 12332−12339.
(45) Hu, C.-M. J.; Fang, R. H.; Wang, K.-C.; Luk, B. T.; Thamphiwatana, S.; Dehaini, D.; Nguyen, P.; Angsantikul, P.; Wen, C. H.; Kroll, A. V.; Carpenter, C.; Ramesh, M.; Qu, V.; Patel, S. H.; Zhu, J.; Shi, W.; Hofman, F. M.; Chen, T. C.; Gao, W.; Zhang, K.; Chien, S.; Zhang, L. Nanoparticle Biointerfacing by Platelet Membrane Cloaking. *Nature* **2015**, *526*, 118−121.
(46) Imai, Y.; Nose, Y. A New Method for Evalution of Antithrombogenicity of Materials. *J. Biomed. Mater. Res.* **1972**, 165.
(47) Nan, H.; Ping, Y.; Xuan, C.; Yongxang, L.; Xiaolan, Z.; Guangjun, C.; Zihong, Z.; Feng, Z.; Yuanru, C.; Xianghuai, L.; Tingfei, X. Blood Compatibility of Amorphous Titanium Oxide Films Synthesized by Ion Beam Enhanced Deposition. *Biomaterials* **1998**, 771.
(48) Shvartsman, D.; Storrie-White, H.; Lee, K.; Kearney, C.; Brudno, Y.; Ho, N.; Cezar, C.; McCann, C.; Anderson, E.; Koullias, J.; Tapia, J. C.; Vandenburgh, H.; Lichtman, J. W.; Mooney, D. J. Sustained Delivery of VEGF Maintains Innervation and Promotes Reperfusion in Ischemic Skeletal Muscles Via NGF/GDNF Signaling. *Mol. Ther.* **2014**, *22*, 1243−1253.
(49) Ungerleider, J. L.; Kammeyer, J. K.; Braden, R. L.; Christman, K. L.; Gianneschi, N. C. Enzyme-Targeted Nanoparticles for Delivery to Ischemic Skeletal Muscle. *Polym. Chem.* **2017**, 5212.
(50) Benton, R. L.; Maddie, M. A.; Minnillo, D. R.; Hagg, T.; Whittemore, S. R. Griffonia Simplicifolia Isolectin B4 Identifies a Specific Subpopulation of Angiogenic Blood Vessels Following Contusive Spinal Cord Injury in the Adult Mouse. *J. Comp. Neurol.* **2008**, 1031.
(51) Murthy, N.; Robichaud, J. R.; Tirrell, D. A.; Stayton, P. S.; Hoffman, A. S. The Design and Synthesis of Polymers for Eukaryotic Membrane Disruption. *J. Controlled Release* **1999**, *61*, 137−143.
(52) Brazel, C. S. Reflexive Polymers and Hydrogels: Understanding and Designing Fast Responsive Polymeric Systems. *J. Am. Chem. Soc.* **2005**, *127*, 1590.
(53) Hu, Q.; Sun, W.; Qian, C.; Wang, C.; Bomba, H. N.; Gu, Z. Anticancer Platelet-Mimicking Nanovehicles. *Adv. Mater.* **2015**, *27*, 7043−7050.
(54) Tang, J.; Su, T.; Huang, K.; Dinh, P.-U.; Wang, Z.; Vandergriff, A.; et al. Targeted Repair of Heart Injury by Stem Cells Fused with Platelet Nanovesicles. *Nat. Biomed. Eng.* **2018**, *2*, 17−26.
(55) Wang, Y.; Lin, T.; Zhang, W.; Jiang, Y.; Jin, H.; He, H.; Yang, V. C.; Chen, Y.; Huang, Y. A Prodrug-Type, MMP-2-Targeting Nanoprobe for Tumor Detection and Imaging. *Theranostics* **2015**, 787.
(56) Kanki, S.; Jaalouk, D. E.; Lee, S.; Yu, A. Y. C.; Gannon, J.; Lee, R. T. Identification of Targeting Peptides for Ischemic Myocardium by in Vivo Phage Display. *J. Mol. Cell. Cardiol.* **2011**, *50*, 841−848.
(57) Wang, X.; Chen, Y.; Zhao, Z.; Meng, Q.; Yu, Y.; Sun, J.; Yang, Z.; Chen, Y.; Li, J.; Ma, T.; Liu, H.; Li, Z.; Yang, J.; Shen, Z. Engineered Exosomes with Ischemic Myocardium-Targeting Peptide for Targeted Therapy in Myocardial Infarction. *J. Am. Heart Assoc.* **2018**, No. e008737.
(58) Nachman, R. L.; Ferris, B. Studies on the Proteins of Human Platelet Membranes. *J. Biol. Chem.* **1972**, *247*, 4468−4475.
(59) Casares, D.; Escribá, P. V.; Rosselló, C. A. Membrane Lipid Composition: Effect on Membrane and Organelle Structure, Function and Compartmentalization and Therapeutic Avenues. *Int. J. Mol. Sci.* **2019**, *20*, No. 2167.
(60) Nguyen, M. M.; Carlini, A. S.; Chien, M. P.; Sonnenberg, S.; Luo, C.; Braden, R. L.; Osborn, K. G.; Li, Y.; Gianneschi, N. C.; Christman, K. L. Enzyme-Responsive Nanoparticles for Targeted Accumulation and Prolonged Retention in Heart Tissue after Myocardial Infarction. *Adv. Mater.* **2015**, *27*, 5547−5552.
(61) Oyewumi, M. O.; Yokel, R. A.; Jay, M.; Coakley, T.; Mumper, R. J. Comparison of Cell Uptake, Biodistribution and Tumor Retention of Folate-Coated and PEG-Coated Gadolinium Nanoparticles in Tumor-Bearing Mice. *J. Controlled Release* **2004**, 613.
(62) Riso, E.-M.; Kaasik, P.; Seene, T. Remodelling of Skeletal Muscle Extracellular Matrix: Effect of Unloading and Reloading. *Composition and Function of the Extracellular Matrix in the Human Body*; IntechOpen, 2016.
(63) Hance, A. J.; Crystal, R. G. Rigid Control of Synthesis of Collagen Types I and III by Cells in Culture. *Nature* **1977**, *268*, 152−154.
(64) Phan, S. H. The Myofibroblast in Pulmonary Fibrosis. *Chest* **2002**, 286S.
(65) Krishna, S. M.; Omer, S. M.; Li, J.; Morton, S. K.; Jose, R. J.; Golledge, J. Development of a Two-Stage Limb Ischemia Model to Better Simulate Human Peripheral Artery Disease. *Sci. Rep.* **2020**, No. 3449.
(66) Muhs, B. E.; Plitas, G.; Delgado, Y.; Ianus, I.; Shaw, J. P.; Adelman, M. A.; Lamparello, P.; Shamamian, P.; Gagne, P. Temporal Expression and Activation of Matrix Metalloproteinases-2, -9, and Membrane Type 1—Matrix Metalloproteinase Following Acute Hindlimb Ischemia. *J. Surg. Res.* **2003**, *111*, 8−15.
(67) Rundhaug, J. E. Matrix Metalloproteinases and Angiogenesis. *J. Cell. Mol. Med.* **2005**, *9*, 267−285.
(68) Levi, E.; Fridman, R.; Miao, H. Q.; Ma, Y. S.; Yayon, A.; Vlodavsky, I. Matrix Metalloproteinase 2 Releases Active Soluble Ectodomain of Fibroblast Growth Factor Receptor 1. *Proc. Natl. Acad. Sci. U.S.A.* **2002**, 7069.
(69) Valarmathi, M. T. *Muscle Cells—Recent Advances and Future Perspectives*; IntechOpen, 2020.
(70) Kluger, M. A.; Zahner, G.; Paust, H. J.; Schaper, M.; Magnus, T.; Panzer, U.; Stahl, R. A. K. Leukocyte-Derived MMP9 Is Crucial for the Recruitment of Proinflammatory Macrophages in Experimental Glomerulonephritis. *Kidney Int.* **2013**, 865.


https://dx.doi.org/10.1021/acsami.0c19271
*ACS Appl. Mater. Interfaces* 2021, 13, 5907−5918